THE ASTROPHYSICAL JOURNAL, 498:26–42, 1998 May 1

WEAK LENSING AND COSMOLOGY

NICK KAISER
Institute for Astronomy, University of Hawaii, 2680 Woodlawn Drive, Honolulu, HI 96822; kaiser@hawaii.edu
Received 1996 October 15; accepted 1997 December 11

ABSTRACT

We explore the dependence of weak lensing phenomena on the background cosmology. We first generalize the relation between $P_\psi(\omega)$, the angular power spectrum of the distortion, and the power spectrum of density fluctuations to nonflat cosmologies. We then compute P_ψ for various illustrative models. A useful cosmological discriminator is the growth of P_ψ with source redshift, which is much stronger in low–matter density models and especially in Λ-dominated models. With even crude redshift information (say from broadband colors), it should be possible to constrain the cosmological world model. The amplitude of $P_\psi(\omega)$ is also quite sensitive to the cosmology, but requires a reliable external normalization for the mass fluctuations. If one normalizes to galaxy clustering, with M/L fixed by small-scale galaxy dynamics, then low-density models predict a much stronger distortion. If, however, one normalizes to large-scale bulk flows, the predicted distortion for sources at redshifts $Z_s \sim 1$–3 is rather insensitive to the background cosmology. The signals predicted here can be detected at a very high level of significance with a photometric survey covering, say, 10 deg^2, but sparse sampling is needed to avoid large sampling variance. We discuss the factors influencing the design of an optimum survey. Turning to weak lensing by clusters, we find that for high lens redshifts ($Z_l \simeq 1$) the critical density is substantially reduced in Λ-models, but that the ratio of the shear or convergence to the velocity dispersions or X-ray temperature of clusters is only very weakly dependent on the cosmology.

Subject heading: cosmology: theory — gravitational lensing — large-scale structure of universe

1. INTRODUCTION

Weak lensing is the distortion of the shapes and sizes (and hence fluxes) of distant galaxies from the tidal deflection of light rays by structures along the line of sight. This provides a powerful probe of mass fluctuations on a wide range of scales from galaxy halos (Valdes et al. 1984; Brainerd, Blandford, & Smail 1996) through clusters (Tyson, Valdes, & Wenk 1990; Bonnet et al. 1993; Bonnet, Mellier, & Fort 1994; Dahle, Maddox, & Lilje 1994; Fahlman et al. 1994; Smail et al. 1994; Smail & Dickinson 1995; Tyson & Fisher 1995; Fort et al. 1996; Squires et al. 1996a, 1996b; Dahle et al. 1996; Fort et al. 1996) to supercluster scales (Valdes, Tyson, & Jarvis 1983; Mould et al. 1994; Villumsen 1996a). As the distortion depends on the distance to the sources—being generally larger for more distant sources—weak lensing also provides a way to constrain the redshift distribution for very faint galaxies (Smail, Ellis, & Fitchett 1995; Luppino and Kaiser 1997; Fort, Mellier, & Dantel-Fort 1996).

The first quantitative predictions for the distortion effect were made by Gunn (1967), who was primarily interested in what limits this placed on the classical cosmological tests. Dyer & Roeder (1974) estimated the distortion using "Swiss cheese" models—with results quite similar to modern estimates (see below)—although they dismissed the effect as too small to have much observational significance. Webster (1985) computed the increase in ellipticity of distant objects in models with strong small-scale mass inhomogeneity. This is related to the weak lensing effects discussed here, although in fact, the broadening of the distribution of ellipticities only appears at second and higher order in the gravitational potential Φ and vanishes in the weak-lensing limit considered here. In weak lensing one considers the galaxy ellipticity to be a two-component vectorlike quantity $e_\alpha = e(\cos 2\varphi, \sin 2\varphi)$, where φ is the position angle. The expectation value of e_α vanishes in the absence of lensing, and one searches for a coherent statistical anisotropy of the e_α distribution caused by intervening matter.

Quantitative predictions for weak lensing from modern *ab initio* models for large-scale structure were made by Blandford et al. (1991) and Miralda-Escudé (1991), who computed the rms distortion or "polarization" of distant galaxy shapes and found that it could be quite large—on the order of a few percent in rms shear—for the then popular theoretical models, such as cold dark matter (CDM), and that the rms shear increased as the 3/2 power of comoving source distance. These works also estimated the shear autocorrelation function. In Kaiser (1992, hereafter K92) this analysis was generalized to include a distribution of source distances and extended in a number of other ways. K92 showed (1) how the angular power spectrum of the shear field was related to the power spectrum of the density fluctuations in three dimensions, (2) that shear at observable levels on degree scales was an inevitable consequence of density fluctuations inferred from large-scale deviations from Hubble flow or "bulk flows (see Strauss & Willick 1995 for a detailed review), (3) that the (Fourier transform of the) projected surface density could be computed from the shear, and (4) that one could determine the mass-to-light ratio for foreground structure by cross-correlating the foreground galaxy density distribution with the shear. However, this analysis, like those of Blandford et al. and Miralda-Escudé, was restricted to the Einstein–de Sitter cosmological background. More recently, Villumsen (1996b) and Bar-Kana (1996) have discussed the distortion in open cosmologies. Here we will explore in more detail how the cosmological background affects weak-lensing observables. In § 2 we give a brief yet self-contained derivation of the distortion tensor, which describes the mapping between angles on the sky at the observer and position on some distant source plane, as a projection of the transverse components of the tidal field along the line of sight. In § 3

we consider lensing by large-scale structure. We first derive the relation between the angular power spectrum of the distortion and the power spectrum of the density fluctuations, and we then consider various illustrative models for $P(\omega)$ and discuss the feasibility of these observations and sampling-strategy issues. In § 4 we consider lensing by individual clusters. Our main goal is to elucidate the dependence of weak lensing phenomena on the background cosmologies; this will enable us to understand to what extent our conclusions about the mass distribution and the redshifts of faint galaxies are cosmology dependent and, to turn the question around, to see to what extent weak-lensing observations, perhaps combined with other observations, can be used to constrain the cosmological world model. In a recent study Bernardeau, van Waerbeke, & Mellier (1996) have also considered some aspects of weak lensing considered here, though their work emphasized more the possibility of measuring higher order moments (than second order).

2. WEAK LENSING IN A FRW COSMOLOGY

We take as the metric for the homogeneous and isotropic FRW background

$$ds^2 = g_{\alpha\beta}\,dr^\alpha\,dr^\beta = -dt^2 + a^2(t)(dz^2 + \sinh^2 z\,d\sigma^2)\,, \quad (1)$$

where $d\sigma^2 \equiv d\theta^2 + \sin^2\theta\,d\varphi^2$. (Here z measures comoving separation; we will use uppercase Z to denote redshift.) This is for the open case; for the closed world model we replace $\sinh z$ with $\sin z$. The curvature radius a obeys

$$\left(\frac{da}{dt}\right)^2 = H_0^2 a_0^2\left(\Omega_m \frac{a_0}{a} + \Omega_\Lambda \frac{a^2}{a_0^2}\right) \pm 1\,, \quad (2)$$

with positive/negative curvature term for open/closed models, and where $H \equiv (da/dt)/a$ is the expansion rate; a subscript zero denotes the present value; and Ω_m, Ω_Λ are understood to be the present values of the density from matter and from the cosmological constant in units of the critical value $\rho_c = 3H_0^2/(8\pi G)$. Evaluating equation (2) at the present, we find that the curvature radius, which we shall use as the scale factor, is related to the current expansion rate by

$$a_0 = \frac{1}{H_0(1-\Omega_0)^{1/2}}\,, \quad (3)$$

where $\Omega_0 \equiv \Omega_m + \Omega_\Lambda$. We will focus on flat and open models (the former being considered as the limiting case of the latter), although it is straightforward to generalize the formulae below to the closed case.

With the addition of small-scale matter inhomogeneity, we can take the metric to be

$$ds^2 = -(1+2\Phi)dt^2 + (1-2\Phi)a^2(t)(dz^2 + \sinh^2 z\,d\sigma^2)\,, \quad (4)$$

which, on scales much less than the curvature scale and in Cartesian coordinates, becomes $ds^2 = a^2(\eta_{\alpha\beta} - 2\Phi\ \delta_{\alpha\beta})dr^\alpha\,dr^\beta$, where $\eta_{\alpha\beta} = \mathrm{diag}\,\{-1, 1, 1, 1\}$, which is the usual weak-field solution for a source $\delta\rho(\boldsymbol{r})$, where Φ satisfies Poisson's equation

$$\nabla^2\Phi = 4\pi G\,\delta\rho\,, \quad (5)$$

and where the Laplacian is taken with respect to proper distance.

Photon trajectories in the spacetime equation (4) are solutions of the geodesic equation

$$\frac{d^2 r^\alpha}{d\lambda^2} = -g^{\alpha\beta}\left(g_{\beta\nu,\mu} - \frac{1}{2}\,g_{\nu\mu,\beta}\right)\frac{dr^\mu}{d\lambda}\,\frac{dr^\nu}{d\lambda}\,. \quad (6)$$

To zeroth order in Φ and for null geodesics, the time component of equation (6) is $d^2t/d\lambda^2 = -H(dt/d\lambda)^2$, which one can solve to obtain the affine parameter $d\lambda = a\,dt$. Let us consider rays confined to a narrow cone around the polar axis, $\theta \ll 1$, and let $d\sigma^2 = d\theta_x^2 + d\theta_y^2$, with $\theta_x = \theta\cos\varphi$ and $\theta_y = \theta\sin\varphi$. The zeroth order solution of the radial component of equation (6) is $dz/d\eta = 1$, where the conformal time is defined as usual by $\eta \equiv \int dt/a$. The angular components of equation (6) (up to first order in Φ) $d\theta_i/d\eta$, are

$$\frac{d^2\theta_i}{d\eta^2} = -2\,\frac{\cosh z}{\sinh z}\,\frac{d\theta_i}{d\eta} - \frac{2}{\sinh^2 z}\,\frac{\partial\Phi}{\partial\theta_i}\,, \quad (7)$$

or, in terms of the transverse comoving displacement of the ray from the polar axis measured in units of the curvature scale, $x_i = \theta_i \sinh z$,

$$\ddot{x}_i = x_i - 2\partial_i\,\Phi(\boldsymbol{x}, z)\,, \quad (8)$$

where $\partial_i \equiv \partial/\partial x_i$, and dots denote differentiation with respect to conformal look-back time z. The first term describes the tendency for neighboring rays to diverge because of the hyperbolic geometry, and it becomes negligible in the limit $\Omega_0 \to 1$, while the extra forcing term is, as usual, just twice the transverse gradient of the Newtonian potential, evaluated along the actual light ray.

The general solution of equation (8) is

$$x_i = A_i \sinh z + B_i \cosh z - 2 \times \int_0^z dz'\,\partial_i\,\Phi[\boldsymbol{x}(z'), z']\,\sinh(z - z')\,, \quad (9)$$

which one can readily verify by direct differentiation. The constants of integration A and B are set by the boundary conditions. For a ray that reaches the observer (whom we shall place at the origin of our coordinates) from direction θ_{0i}, these conditions are $B_i = 0$ and $A_i = \theta_{0i}$.

Equation (9) is an implicit equation for $x_i(z)$, but it can be used to generate an explicit solution for $x_i(z)$ as an expansion in powers of the Newtonian potential (which is empirically known to be a very small number for all observed structures in our universe). To zeroth order in Φ, we simply have $x_i^{(0)} = \theta_{0i}\sinh z$. If we substitute this on the right-hand side of equation (9), we obtain the solution, accurate to first order in Φ,

$$x_i^{(1)} = \theta_{0i}\sinh z - 2\int_0^z dz'\,\partial_i\,\Phi(\boldsymbol{\theta}_0 \sinh z', z')\sinh(z - z')\,, \quad (10)$$

and one can continue this procedure to generate solutions for the photon trajectories of arbitrary accuracy.

If we now consider a pair of neighboring rays that arrive at the observer with directions differing by an infinitesimal angle $\Delta\theta$, then assuming continuity of the potential Φ, we find at the lowest nontrivial order in Φ,

$$\Delta x_i = \Delta\theta_i \sinh z - 2\,\Delta\theta_j \times \int_0^z dz'\,\sinh(z')\sinh(z - z')\partial_j\,\partial_i\,\Phi\,. \quad (11)$$

Equation (11) gives the mapping between angles at the observer and distance on some distant source plane at z_s:

$$\Delta x_l(z_s) = (\delta_{lm} - \psi_{lm}) \sinh z_s \Delta\theta_m , \quad (12)$$

where we have defined the distortion tensor as

$$\psi_{lm}(z_s) = 2 \int_0^{z_s} dz \frac{\sinh z \sinh (z_s - z)}{\sinh z_s} \partial_l \partial_m \Phi , \quad (13)$$

in agreement with Bar-Kana (1996).

At this level of approximation we are effectively computing the deviation of bundles of light rays using the tidal force computed from the unperturbed ray separation and also evaluated along the unperturbed path. This is valid in the limit of vanishingly small distortions, or in the "thin lens" limit, where the ray focusing may become large at great distances, but where the change in the separation of the rays as they pass through the lens is small. One can carry out the expansion in powers of Φ outlined above to the next higher order to quantify the error in this approximation. One finds that the fractional error incurred from using the unperturbed separation is on the order of the distortion itself. As we shall see, for realistic models the expected distortion (for sources at redshift = 3 or thereabouts) is almost certainly less than a few percent, so this source of error is quite small. The fractional error incurred in evaluating the tide along the unperturbed path can, in certain circumstances, be somewhat larger; especially if one is interested in the distortion from small-scale structure, where larger structures can deflect the beam by a substantial fraction of the small-scale coherence length and give a formally larger error. However, we are really interested in rms quantities evaluated along paths through the randomly fluctuating density field, and it can be shown that the real error in such quantities as the two-point function of the distortion are again no larger than the distortion itself.

The distortion tensor ψ_{lm} is an observable quantity, the traceless parts of ψ causing distortion of shapes of distant galaxies and the trace causing amplification and hence modulation of the counts of galaxies. In reality, we deal with the mean distortion tensor averaged over $n(z)$, the distribution of distances to the galaxies

$$\psi_{lm} = \int dz_s n(z_s) \psi_{lm}(z_s) = \int dz g(z) \partial_l \partial_m \Phi , \quad (14)$$

where

$$g(z) \equiv 2 \sinh z \int_z^\infty dz' n(z') \frac{\sinh (z' - z)}{\sinh z'} \quad (15)$$

is a bell-shaped function that peaks at roughly one-half of the background source distance, and where we have normalized $n(z)$ so that $\int dz n(z) = 1$.

3. LARGE-SCALE STRUCTURE

We now consider lensing by large-scale structure. We first derive an expression for the angular power spectrum of some projected quantity (be it galaxy counts, image distortion, etc.) and the corresponding spatial power spectrum. This is the Fourier space analogue of Limber's equation (K92), here generalized to hyperbolic geometries. We then consider various illustrative models for $P(\boldsymbol{k})$ of increasing degrees of realism and then discuss the feasibility of these observations, sampling strategy, and the prospects for probing large-scale structure via the amplification, rather than shear.

3.1. *Limber's Equation in Fourier Space*

A common problem in astronomy is that one observes some quantity on the sky that is the projection of some three-dimensional random field or point process, and one would like to infer the statistical properties of the latter from the former. An example is galaxy clustering, for which one would like to relate, e.g., the angular correlation function of the galaxy counts $w_g(\boldsymbol{\theta})$ to the spatial correlation function $\xi_g(\boldsymbol{\theta})$. The solution to this was given by Limber (1954). Let the projected field be

$$F(\boldsymbol{\theta}) = \int dz q(z) f(\theta_x \sinh z, \theta_y \sinh z, z) , \quad (16)$$

where f is the spatial field written as a function of comoving coordinates (all in units of the curvature scale), and $q(z)$ is some radial weighting function. The angular two-point function of F is

$$w_F(\Delta\boldsymbol{\theta}) = \langle F(\boldsymbol{\theta}) F(\boldsymbol{\theta} + \Delta\boldsymbol{\theta}) \rangle = \int dz \int dz' q(z) q(z') \langle ff' \rangle$$
$$\simeq \int dz q^2(z) \int dz' \xi_f(\Delta\theta_x \sinh z', \Delta\theta_y \sinh z', z'; z) , \quad (17)$$

where $\xi_f(\boldsymbol{r}, z)$ is the spatial two-point function of the field f at lag $\boldsymbol{r}$ and conformal look-back time z, and we have assumed that $q(z)$ is slowly varying compared to the scale of the density fluctuations of interest, and also that these fluctuations occur on a scale much smaller than the curvature scale. This is Limber's (1954) equation, which expresses w_F as an integral of the spatial two-point function. If we Fourier transform equation (17), we obtain the angular power spectrum $P_F(\boldsymbol{\omega})$. If we define the transforms

$$F(\boldsymbol{\omega}) = \int d^2\theta F(\boldsymbol{\theta}) e^{-i\boldsymbol{\omega} \cdot \boldsymbol{\theta}} ,$$
$$f(\boldsymbol{k}) = \int d^3 r f(\boldsymbol{r}) e^{-i\boldsymbol{k} \cdot \boldsymbol{r}} , \quad (18)$$

then under the assumption that the fields F, f are statistically homogeneous [or more specifically that the two-point function $\xi_f = \langle f(\boldsymbol{r}) f(\boldsymbol{r}') \rangle$ depends only on separation $\boldsymbol{r}' - \boldsymbol{r}$], we have

$$\langle F(\boldsymbol{\omega}) F^*(\boldsymbol{\omega}') \rangle = (2\pi)^2 \delta(\boldsymbol{\omega} - \boldsymbol{\omega}') P_F(\boldsymbol{\omega}) ,$$
$$\langle f(\boldsymbol{k}) f^*(\boldsymbol{k}') \rangle = (2\pi)^3 \delta(\boldsymbol{k} - \boldsymbol{k}') P_f(\boldsymbol{k}) , \quad (19)$$

where $P_F(\boldsymbol{\omega})$ and $P_f(\boldsymbol{k})$ are the transforms of $w_F(\boldsymbol{\theta})$ and $\xi_f(\boldsymbol{r})$, so from equation (17),

$$P_F(\boldsymbol{\omega}) = \int d^2\theta\, w_F(\boldsymbol{\theta}) e^{-i\boldsymbol{\omega} \cdot \boldsymbol{\theta}} = \int \frac{d^3k}{(2\pi)^3} P_f(\boldsymbol{k}) \int dz\, q^2(z)$$
$$\times \int d^2\theta\, e^{-i(\omega_x - k_x \sinh z)\theta_x} e^{-i(\omega_y - k_y \sinh z)\theta_y} \int dz'\, e^{-ik_z z'} . \quad (20)$$

The angular and z' integrals here are δ-functions that pick out the particular spatial frequency $\boldsymbol{k} = (\omega_x/\sinh z, \omega_y/\sinh$

z, 0) and that contribute to the angular power at frequency $\omega = (\omega_x, \omega_y)$. Then, invoking the assumed statistical isotropy of $P_f(\boldsymbol{k})$, we have

$$P_F(\omega) = \int dz \, \frac{q^2(z)}{\sinh^2 z} \, P_f\left(\frac{\omega}{\sinh z, z}\right). \tag{21}$$

This is the Fourier space version of Limber's equation and is somewhat simpler than equation (17), as it gives the angular power spectrum of F as a single integral of the spatial power spectrum of f and provides the generalization of equation (A9) of K92 to hyperbolic geometries. As in flat space, it can be thought of as a convolution in log-frequency space of the three-dimensional power spectrum of f. Equation (21) can be used to relate the angular power spectrum of galaxy counts to the three-dimensional spectrum of galaxy clustering, in which context F and f would be the density contrast of galaxies on the sky and in space, and $q(z)$ would be the normalized distribution of galaxy distances $n(z)$. Given a specific prediction for $P(\boldsymbol{k})$, equation (21) enables one to predict $P(\omega)$, or, given a sufficiently high signal-to-noise ratio, one can deconvolve $P(\boldsymbol{k})$ from $P(\omega)$ (see Baugh & Efstathiou 1994, who used this to extract the three-dimensional power spectrum of galaxy clustering $P_g(\boldsymbol{k})$ from the angular power spectrum $P_g(\omega)$ from the Automatic Plate Measuring Facility [APM] survey).

What is the advantage of angular power spectrum analysis (PSA) over the angular autocorrelation function? One minor advantage, as we have seen, is that the former is somewhat easier to compute from $P(\boldsymbol{k})$, particularly when there is evolution of $P(\boldsymbol{k})$. The real advantage of PSA for galaxy clustering, however, is that it is easy to compute the real uncertainty in the power estimates, and that the error matrix for $P(\omega)$ is nearly diagonal. Aside from a readily calculable short-range correlation on scales $\delta\omega \sim 1/\Theta$, where Θ is the dimension of the survey, estimates of $P(\omega)$ at different frequencies are statistically independent. Neither of these pleasant properties holds for correlation analysis. In weak lensing, as we shall now see, there is a further advantage in that the observable is a symmetric 2×2 tensor, and there are various correlation functions one can form; making sense of the interrelation between these is much simpler in terms of power spectra.

3.2. *Power Spectrum of the Distortion*

It is now very easy to compute the power spectrum of the distortion $P_\psi(\omega)$ in terms of the three-dimensional density-field power spectrum $P(\boldsymbol{k})$, or equivalently, in terms of $P_\Phi(\boldsymbol{k})$, the power spectrum for the potential fluctuations.

The distortion tensor equation (14) can be written as the second derivative of a "projected potential":

$$\psi_{lm}(\boldsymbol{\theta}) = \partial_l \partial_m \Phi_p(\boldsymbol{\theta}) \, , \tag{22}$$

where ∂_l here (and henceforth) denotes $\partial/\partial\theta_l$, and where

$$\Phi_p(\boldsymbol{\theta}) = \int dz \, \frac{g(z)}{\sinh^2 z} \, \Phi(\theta_x \sinh z, \theta_y \sinh z, z) \, , \tag{23}$$

which is in the form of equation (16), with $q = g/\sinh^2 z$. In Fourier space, differentiation is equivalent to multiplication by $i\omega$: $\partial_l \Phi_p \rightarrow i\omega_l \Phi_p$, so $\psi_{lm}(\omega) = -\omega_l \omega_m \Phi_p(\omega)$. The two-point function for the distortion is therefore

$$\langle \psi_{ij}(\omega) \psi^*_{lm}(\omega') \rangle = (2\pi)^2 \delta(\omega' - \omega) \hat{\omega}_i \hat{\omega}_j \hat{\omega}_l \hat{\omega}_m P_\psi(\omega) \, , \tag{24}$$

which nicely factorizes into a pure angular term involving the unit wavevector $\hat{\omega}$—which, as we will discuss below, can be used as a test of the integrity of the data—and the "distortion power spectrum":

$$P_\psi(\omega) = \omega^4 \int dz \, \frac{g^2(z)}{\sinh^6 z} \, P_\Phi\left(\frac{\omega}{\sinh z, z}\right), \tag{25}$$

which is a function only of ω. Equation (25) expresses $P_\psi(\omega)$ as a convolution in log-frequency space of the power spectrum of potential fluctuations $P_\Phi(k)$ or equivalently to the power spectrum of density fluctuations $P_\delta(k)$, which is related to $P_\Phi(k)$ through Poisson's equation (see eq. [34] below). Villumsen (1996b) has obtained an expression similar to equation (25), but finds a different angular dependence.

3.3. *Models for $P_\Psi(\omega)$*

We now compute $P_\Psi(\omega)$ for various models for the three-dimensional power spectrum $P_\Phi(k)$. We first consider the effect of power concentrated at a single spatial frequency. We next consider power-law models, and finally, we consider empirical models that seem to fit most of the data on galaxy clustering as constructed by Peacock (1996).

3.3.1. *δ-Function $P(\boldsymbol{k})$*

To explore how the background cosmology affects the interpretation of $P_\psi(\omega)$, let us first compute the angular power spectrum for a narrow band of power at some frequency with present physical wavenumber $k_{\rm phys} = k_*$, i.e., $P_\phi(k) = 2\pi^2 \langle \Phi^2 \rangle (a_0 k_*)^{-2} \delta(k - a_0 k_*)$. Inserting this in equation (25) and considering the effect on sources at a single distance [$n(z) \rightarrow \delta(z - z_s)$, so $g(z) \rightarrow 2 \sinh z \sinh (z_s - z)/\sinh z_s$], we find

$$P_\psi(\omega) = 8\pi^2 \langle \Phi^2 \rangle \omega \, \frac{f^2(z) \sinh^2 (z_s - z)}{\sinh^2 z_s \cosh z} \, , \tag{26}$$

where $z = \sinh^{-1} [\omega/(a_0 k_*)]$, and P_ψ vanishes for $\omega > a_0 k_* \sinh z_s$. Here $f = (a_0/a)(\delta/\delta_0)$ is the growth factor for the potential, expressed as a function of look-back time. Equation (26) is calculated as follows: Equation (2) gives H/H_0 as a function of $1 + Z = a_0/a$. Starting at some very high redshift, we compute $\eta = \int dt/a = \int da \, H/a$ to obtain the conformal look-back time $z = \eta_0 - \eta$ as a function of Z. We also integrate the equation for the growth of density perturbations,

$$\frac{d^2\delta}{dt^2} + 2H \frac{d\delta}{dt} - G\rho_m \delta = 0 \, , \tag{27}$$

to obtain δ/δ_0 for the growing mode. The result is shown for three representative cosmological models in Figure 1. In all cases, the angular power spectrum is a bell-shaped curve, peaking at roughly $\frac{1}{2}$ the maximum angular frequency $\omega_{\rm max} = a_0 k_* \sinh z_s$. Furthermore, the total power increases quite rapidly with increasing source redshift, this trend being strongest for the Λ-dominated models.

In Figure 2 we show the total power

$$\int \frac{d\omega}{2\pi} \omega P_\psi(\omega) = 4\pi \langle \Phi^2 \rangle \left(\frac{k_*}{H_0}\right)^3 (1 - \Omega_0)^{-3/2} \times \int_0^{z_s} dz f^2(z) \frac{\sinh^2 z \sinh^2 (z_s - z)}{\sinh^2 z_s} \, , \tag{28}$$

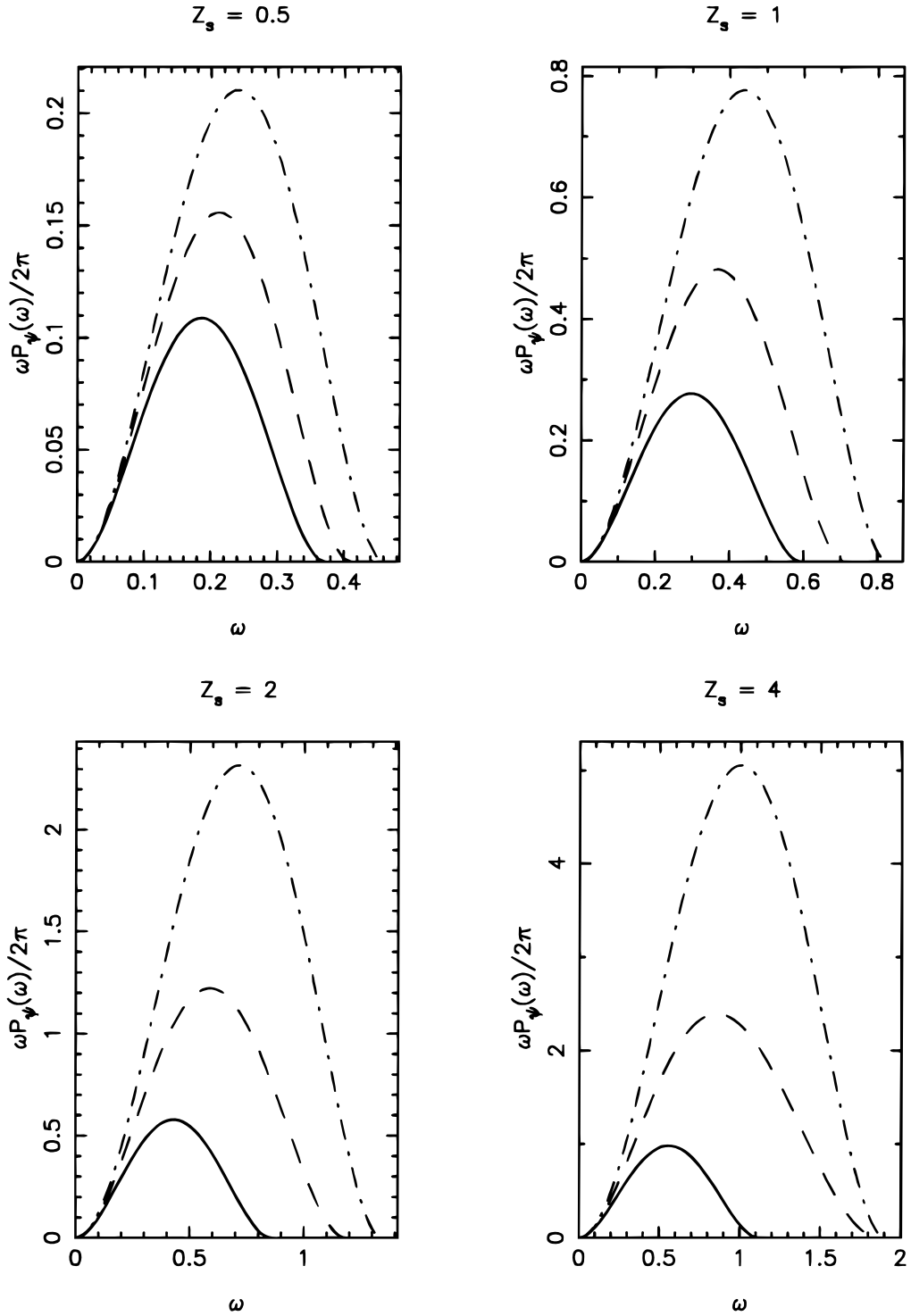

FIG. 1.—Angular power spectra for a δ-function spatial power spectrum and for various source redshifts. We have used $\omega P_\psi(\omega)/2\pi$ as ordinate (with linear frequency as the abscissa), so that the area under the curves represents the total power. The solid line is the EdS model; the dashed line is an open $\Omega_m = 0.2$ model; and the dash-dotted line is a Λ-dominated model, also with $\Omega_m = 0.2$. The numerical values are for $\langle\Phi^2\rangle = 1$, $k_* = H_0$, so for any other values, the vertical and horizontal scales should be multiplied by $\langle\Phi^2\rangle(k_*/H_0)^2$ and k_*/H_0, respectively. Note the gross difference in vertical scale for the various plots.

and the mean (power-weighted) angular frequency

$$\bar{\omega} \equiv \frac{\int d\omega\omega^2 P_\psi(\omega)}{\int d\omega\omega P_\psi(\omega)}\,, \tag{29}$$

as a function of source redshift. At low source redshift the distortion power spectrum is essentially independent of the background cosmology, as one might expect, but at high Z_s the low–matter density models predict higher distortion. This results in part from the fact that Φ decreases with time in these models and in part from the greater path length back to a given source redshift.

3.3.2. *Power-Law P(k)*

These results for a δ-function $P_\Phi(k)$ are most useful for showing what spatial scales we are probing when we measure the angular power at some frequency. For a realistic $P_\Phi(k)$ we will see a blend of angular spectra of the form of

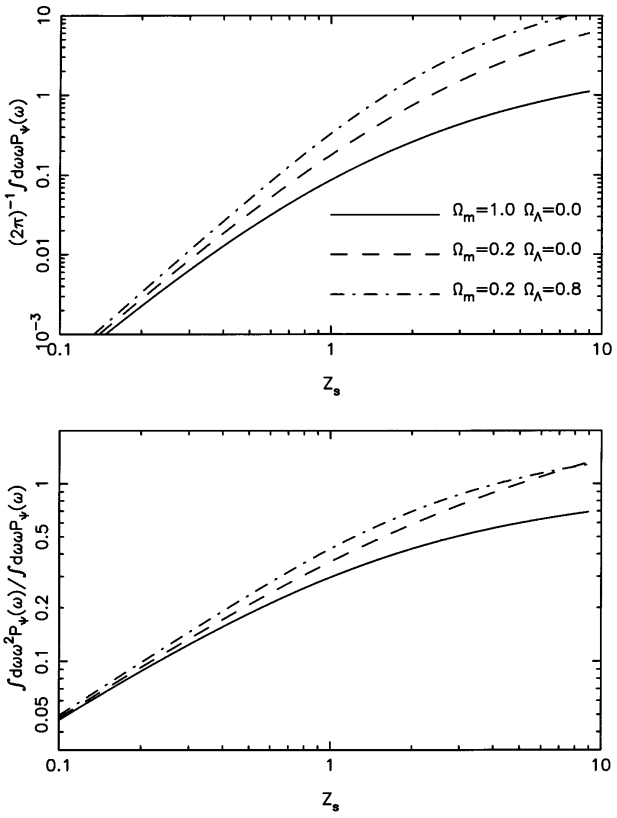

FIG. 2.—Upper panel shows the total distortion power (for a δ-function potential power spectrum) as a function of the source redshift. As before, the numerical values assume $\langle\Phi^2\rangle = 1$, $k_* = H_0$, and one should multiply the vertical scale by $\langle\Phi^2\rangle(k_*/H_0)^3$ for other values. The lower panel shows the power-weighted mean angular frequency for a fiducial physical wavenumber $k_* = H_0$, which shows that in low–matter density models, the power from a given physical scale appears at a somewhat (up to about a factor of 2) larger angular frequency. More striking, however, is the difference in the total power between the models; low–matter density models, and especially Λ-models, predict much stronger distortion. The same amplitude of three-dimensional potential fluctuations is assumed for the different cosmologies. The motivation for this and alternative normalizations are discussed in the text.

equation (26). As a next step toward realism, we now model $P_\Phi(k)$ as a power law $P_\Phi(k) \propto k^{n-4}$ (following the usual convention that the density power spectrum scales as k^n). To set the normalization consistently (corresponding to a given metric fluctuation variance on a given physical scale), let us take

$$\frac{k^3 P_\Phi(k)}{2\pi^2} = \langle\Phi^2\rangle_* \left(\frac{k_{\rm phys}}{k_*}\right)^{n-1} = \langle\Phi^2\rangle_* \left(\frac{k}{a_0 k_*}\right)^{n-1}, \quad (30)$$

so that $\langle\Phi^2\rangle_*$ is the contribution to the variance of the potential per log interval of angular wavenumber at some fiducial (physical) wavenumber k_*. For the distortion power per log interval of wavenumber, this gives

$$\frac{\omega^2 P_\psi(\omega)}{(2\pi)} = 4\pi C_n(z_s)\langle\Phi^2\rangle_* \left(\frac{k_*}{H_0}\right)^{1-n} \omega^{2+n}, \quad (31)$$

where the cosmology dependence is all hidden in the function

$$C_n(z_s) = (1-\Omega_0)^{(n-1)/2} \int_0^{z_s} dz f^2(z) \frac{\sinh^2(z_s - z)}{\sinh^n z \sinh^2 z_s}. \quad (32)$$

Note that for $n = -2$, which gives equal variance in ψ per log interval of wavenumber, equations (31) and (32) are essentially identical to equation (28). The dependence of $P_\psi(\omega)$ on source redshift is shown in Figure 3 for various values of the spectral index n.

3.3.3. *Normalization*

It is readily apparent that the distortion power is a strongly increasing function of source redshift in all cosmologies (though the trend is n-dependent). We also see that the predicted distortion for high-Z sources is sensitive to the cosmology, with low–matter density models—and Λ-models in particular—giving a much stronger predicted signal. This might seem to be at odds with the conclusions of Villumsen (1996a) and Bernardeau et al. (1996), both of whom find the distortion to be a strongly *increasing* function of Ω_m (Bernardeau et al. 1996 find variance for the top-hat averaged shear approximately proportional to $\Omega_m^{1.5}$, for instance). However, the difference is simply one of normalization; we have normalized to a given rms potential fluctuation, whereas Villumsen and Bernardeau et al. have implicitly normalized to a given rms density contrast; had we done so, it would have reduced our predictions by a factor Ω_m^2. The question of what the appropriate normalization may be is an interesting one, and one to which there is as yet no completely definitive answer. Were it the case that all one knew about the universe was the galaxy correlation function ξ_g, then one could reasonably make a case for normalizing to a given density contrast, implicitly assuming, in the absence of any evidence to the contrary, that galaxies are unbiased tracers of the mass. However, there is actually a wealth of data from dynamical studies of various kinds to suggest that the appropriate normalization for the density contrast is quite strongly Ω_m dependent; in high-Ω models the galaxy distribution must be biased, and it makes sense to incorporate this into one's predictions for the rms distortion.

One line of evidence comes from small-scale pairwise velocities; in the regime where these motions are in equilibrium, these measure the present potential fluctuations directly and would therefore lead one to normalize as we have done. Thus, if one assumes a scale-independent bias, with M/L tied to small-scale "cosmic virial theorem" measurements (Davis & Peebles 1983), then, as shown in Figure 3, low-Ω_m models predict much stronger distortion at high Z_s. (This assumes that one is using "real-space" estimates of ξ_g; if one uses redshift survey–based estimates, one should allow for the boosting of power caused by streaming motions; Kaiser 1987.) Another line of evidence comes from peculiar velocities on large scales: the so-called bulk flows (e.g., Strauss & Willick 1995 and references therein). The advantage of these observations is that they directly probe the mass and give a normalization to the mass fluctuations on large scales, where, as we shall see, we expect weak lensing to be most powerful. The disadvantage is that they are very hard to measure reliably, and estimates of the mass power spectrum derived therefrom have very large sampling uncertainty, as the observations typically probe only a few independent fluctuation volumes. Here the velocity on a given scale is, crudely speaking, given by the potential gradient times the age of the universe, and as the latter is greater in low-Ω_m models, we would infer a lower potential fluctuation amplitude for a given amplitude for the streaming motions. A detailed analysis shows that this reduces the

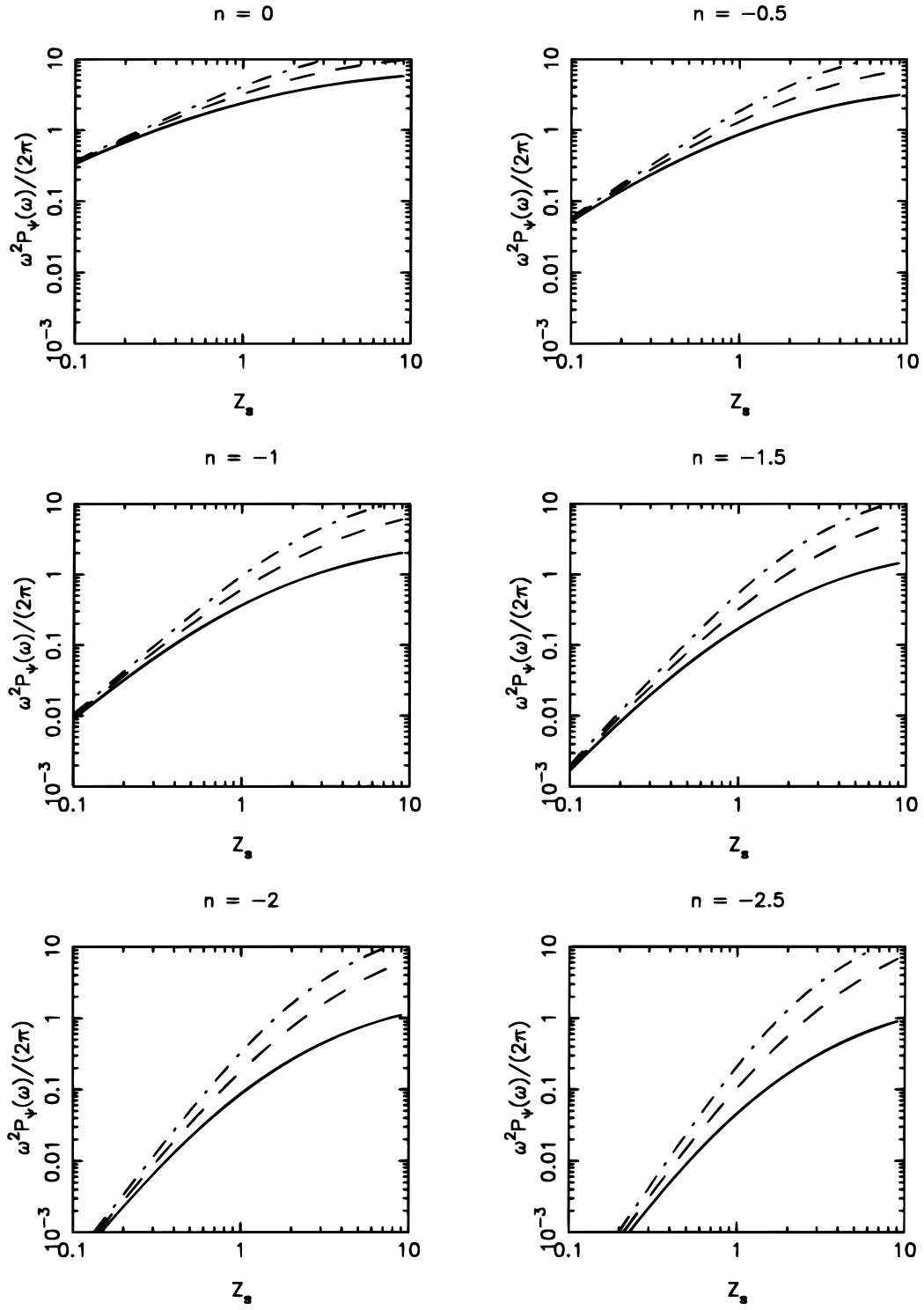

FIG. 3.—Dependence of the power (per log interval of wavenumber) on source redshift for our three example cosmological models, now assuming a power-law spectrum of density fluctuations. The quantity plotted here is actually $4\pi C_n$ and should be multiplied by $\langle\Phi^2\rangle_*(k_*/H_0)^{1-n}w^{2+n}$ to obtain the real power per log interval of angular wavenumber.

predicted distortion by roughly a factor of $\Omega_m^{0.4}$ for low-Ω_m models (in amplitude, that is, corresponding to a factor $\Omega_m^{0.8}$ in power). The predicted distortion power is shown in Figure 4 for this normalization. Now we find that the greatest distinction between models appears at very low source redshift, but for sources at $Z_s \sim 1$–3 and realistic spectral indices, the predictions are only mildy dependent on cosmology and hence on Ω_m. A third line of evidence comes from the abundance of clusters as a function of velocity dispersion or X-ray temperature. With, e.g., the Press-Schechter (1974) model for the mass function, these data can be used to normalize the amplitude of mass fluctuations (Cole & Kaiser 1989). In high-Ω models and with the best current data, this gives $\sigma_8 \sim 0.57\Omega_m^{-0.56}$ (White, Efstathiou, & Frenk 1993), which is very similar to the scaling from peculiar velocities. However, since low-density models tend to produce power spectra with more large-scale power (as the horizon size at matter-radiation equality is increased),

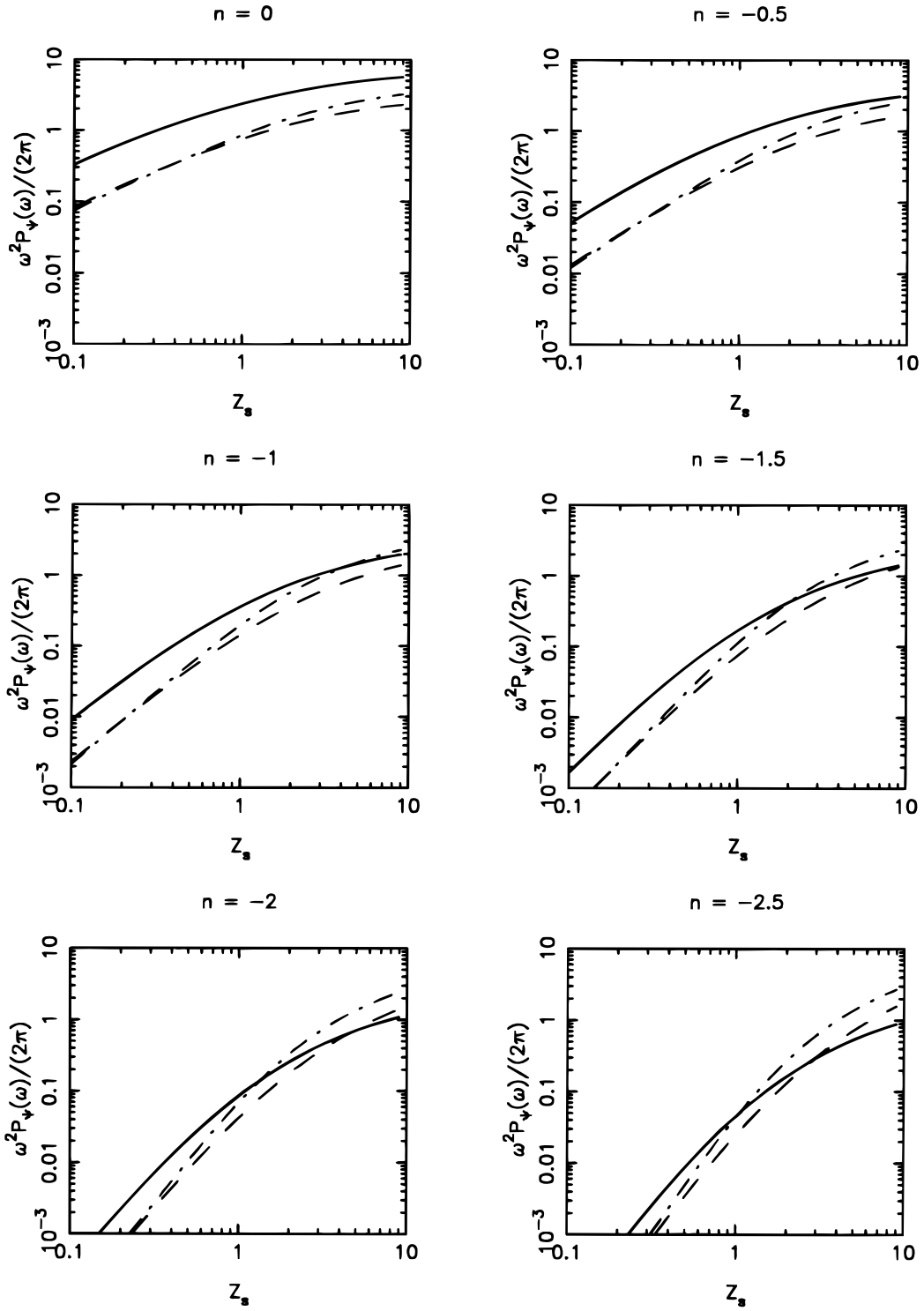

FIG. 4.—Predicted distortion power vs. source redshift, as in Fig. 3, but normalized assuming a fixed amplitude of bulk flows

the predicted power at large scales in low-Ω_m models would not be suppressed as much as with the bulk-flow normalization, and one would expect to find something intermediate between the predictions shown in Figures 3 and 4.

There is still considerable uncertainty in the measurements mentioned above and in their interpretation, and there is therefore considerable slop in the predicted distortion. However, we would stress that with any of the normalization methods described above and for sources at reasonably high redshift, i.e., $Z_s \sim 1$–3, and for plausible spectral indices n in the range -1 to -2, say, the Λ-model predictions are at least as high as in the Einstein–de Sitter model, and in open models the predicted distortion power is reduced by at most a factor of 2, and certainly not by a factor of $\Omega^{-1.5}$.

3.3.4. *Empirical Models for P(k)*

As a final example, we give the distortion power predicted according to Peacock's (1996) model for the linear power spectrum, which for high Ω_m incorporates a mild but plaus-

ible level of bias and gives a very good fit to most galaxy clustering data. Poisson's equation (5) gives $P_\Phi(\boldsymbol{k}) = (4\pi)^2 a_0^4 k^{-4} P_\rho(\boldsymbol{k}) = (9/4)\Omega_m^2 k^{-4}(1-\Omega_0)^{-2} P_\delta(\boldsymbol{k})$, where $P_\delta(\boldsymbol{k})$ is the power spectrum for (mass) density contrast, in terms of which equation (25) becomes

$$P_\psi(\omega) = \frac{9\pi^2\Omega_m^2}{2\omega^3}\int dz\,\frac{g^2(z)\,\sinh\, zf^2\Delta^2}{(1-\Omega_0)^2}\,, \qquad (33)$$

where $\Delta^2 \equiv k_{\rm phys}^3 P_\delta^{\rm phys}(k_{\rm phys})/2\pi^2$ is the density contrast power per log interval of wavenumber and should be evaluated at $k_{\rm phys} = \omega H_0(1-\Omega_0)^{1/2}/\sinh\, z$ and at conformal look-back time z. For sources at a single redshift this becomes

$$P_\psi(\omega) = \frac{18\pi^2\Omega_m^2}{\omega^3}\int_0^{z_s} dz\,\frac{\sinh^3\, z\,\sinh^2\,(z_s - z) f^2\Delta^2}{(1-\Omega_0)^2\,\sinh^2\, z_s}\,. \qquad (34)$$

This, or more generally, equations (15) and (33), are the most convenient form if one wishes to predict the distortion from, e.g., *COBE* normalized *ab initio* models. Results are shown in Figure 5 for Peacock's model for $\Delta^2(k)$, which are quite similar in form to mixed dark matter models. Again, we see that the difference between the different cosmological

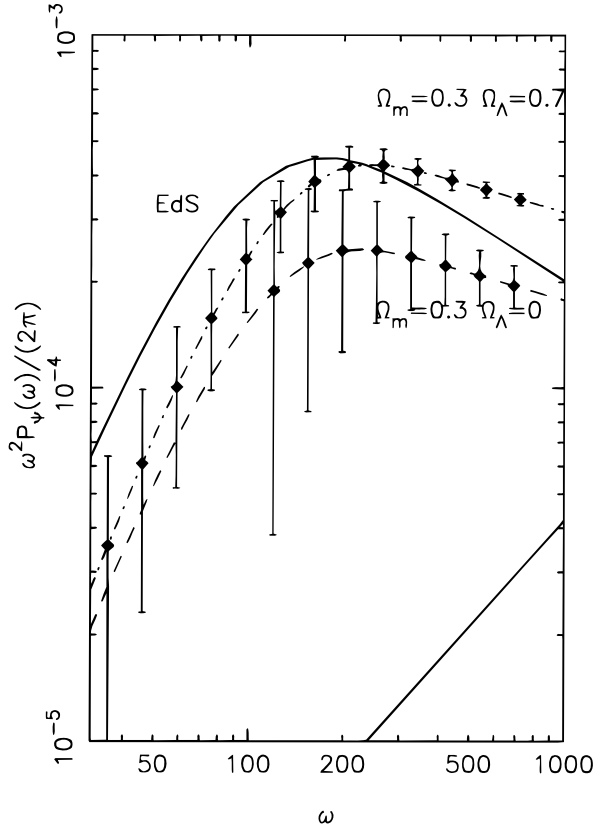

FIG. 5.—Distortion power according to Peacock's (1996) model for $P(k)$; $Z_s = 3$. As before, the solid, dashed, and dash-dotted lines are for EdS, open, and Λ-models, but here the low-density models have $\Omega_m = 0.3$. These predictions are based on a linearized power spectrum. This should be valid at large scales (the strongest distortion here derives from fluctuations with wavelengths $\sim 100\ h^{-1}$ Mpc that are quite accurately linear), but it will tend to underestimate the distortion at small scales, where nonlinearity acts to boost the power considerably at late times. The straight solid line is the expected noise (1 σ) resulting from measurement errors for a 3 deg^2 survey with realistic number density and intrinsic ellipticities as described in the text and for a resolution $d\ln\omega = 0.25$. The large error bars (arbitrarily attached to the open-model prediction) illustrate the sampling noise for a 3° survey at this resolution. These can be reduced considerably by sparse sampling, as illustrated by the error bars attached to the Λ-model, which are for a sparse sample of side = 9°.

models, when normalized realistically, is quite minor. The quantity plotted here is Δ_ψ^2, the contribution to the variance of the trace of ψ_{lm} per log interval, which is 4 times the variance in the shear γ or the convergence κ, so these models are predicting rms shear, convergence $\simeq 1\%$ for $\omega \gtrsim 100$. This is similar to the predictions of K92, although in fact the mass fluctuations assumed here are somewhat lower, while the adopted redshift is higher to reflect the growing evidence (both from lensing and spectroscopy) of a significant high-redshift component at the relevant magnitude limits.

The formalism that we have developed allows us to compute the corresponding quantities for any given distribution function for the background galaxy distances, but, generally speaking, the results are very similar to the single–source plane results for a single plane at the median distance (see, e.g., K92 for examples).

3.4. *Feasibility and Strategy*

We have computed the power spectrum for the distortion tensor ψ_{lm}. The quantities we actually measure are the convergence and shear

$$\kappa = \tfrac{1}{2}\psi_{ll}\,, \quad \gamma_\alpha = \tfrac{1}{2}M_{\alpha lm}\psi_{lm}\,, \qquad (35)$$

where

$$M_{1lm} = \begin{bmatrix} 1 & 0 \\ 0 & -1 \end{bmatrix}, \quad M_{2lm} = \begin{bmatrix} 0 & 1 \\ 1 & 0 \end{bmatrix}. \qquad (36)$$

The shear γ_α is measured from the shapes of galaxies, while the convergence κ can be measured directly from the modulation of the counts. The latter tends to be relatively noisy (see Kaiser et al. 1994), so we will focus, for the moment, on the shear.

3.4.1. *Shear-based $P_\psi(\omega)$*

A procedure for estimating the power spectrum $P_\psi(\omega)$ was outlined in K92. That analysis assumed a simple square survey geometry. Here we will generalize this to more complex survey shapes. Let us assume that we have observations of a set of N galaxies with positions $\{\boldsymbol{\theta}_g\}$, and that we have measured their shapes to obtain a set of properly calibrated shear estimates, i.e., each galaxy provides an estimate $\hat\gamma_\alpha = \gamma_\alpha(\boldsymbol{\theta}_g) + \gamma_\alpha^{\rm int}$, where $\gamma_\alpha^{\rm int}$ is a measure of the random intrinsic ellipticity of the galaxy plus measurement error. The first step is to take the Fourier transform of this set of shear estimates: $\tilde\gamma_\alpha(\omega) = \sum \hat\gamma_\alpha \exp(-i\omega\cdot\theta)$, which we can write as

$$\tilde\gamma_\alpha(\omega) = \int d^2\theta n(\boldsymbol{\theta})\gamma_\alpha(\boldsymbol{\theta}) e^{-i\boldsymbol{\omega}\cdot\boldsymbol{\theta}} + \sum \hat\gamma_\alpha^{\rm int} e^{i\boldsymbol{\omega}\cdot\boldsymbol{\theta}}\,, \qquad (37)$$

where we have introduced $n(\boldsymbol{\theta}) \equiv \sum \delta(\boldsymbol{\theta} - \boldsymbol{\theta}_g)$. Next, we convert this to an estimator of the dimensionless surface density $\tilde\kappa$ as follows: From equations (35) and (22) it follows that the gradients of the surface density and shear are related by $\partial_l \kappa = M_{\alpha lm}\partial_m \gamma_\alpha$ (Kaiser 1995) and hence that $\nabla^2\kappa = M_{\alpha lm}\partial_l\partial_m\gamma_\alpha$, or, in Fourier space, $\kappa(\omega) = M_{\alpha lm}\hat\omega_l\hat\omega_m\gamma_\alpha(\omega)$, which suggests the estimator

$$\tilde\kappa(\omega) = M_{\alpha lm}\hat\omega_l\hat\omega_m\tilde\gamma_\alpha(\omega) = c_\alpha(\omega)\tilde\gamma_\alpha(\omega)\,, \qquad (38)$$

where we have defined $c_\alpha \equiv (\cos 2\varphi, \sin 2\varphi)$, and where φ is in turn defined by $\omega_i = (\omega\cos\varphi, \omega\sin\varphi)$. If one takes the inverse transform of equation (38), one obtains the surface density estimator of Kaiser & Squires (1993). Here we will

use equation (38) to obtain an estimate of the power spectrum P_ψ. From equations (38), (35), (36), and (24) we find

$$\langle|\tilde{\kappa}(\omega)|^2\rangle = N\langle\gamma_1^2\rangle + c_\alpha(\omega)c_\beta(\omega) \times \int \frac{d^2\omega'}{(2\pi)^2}\frac{P_\psi(\omega')}{4} c_\alpha(\omega')c_\beta(\omega')|n(\omega-\omega')|^2 , \quad (39)$$

so $\langle|\tilde{\kappa}|^2\rangle$ does indeed provide an estimate of the power convolved with $|n(\omega)|^2$ plus a constant "shot noise" term $N\langle\gamma_1^2\rangle$, where $\langle\gamma_1^2\rangle$ is the mean-square shear estimate (per component) caused by random intrinsic shapes and measurement error.

For a uniformly sampled square survey geometry of side Θ, the convolving kernel is $|n(\omega)|^2 = N^2 \sin c^2(\omega_x\Theta/2) \sin c^2(\omega_y\Theta/2)$, which falls off rapidly for $\omega \gg \Theta$ (and one could imagine introducing a weight function tapering toward the edge of the box to apodize the kernel further). For realistic spectra and for estimates of the power at $\omega \gg 1/\Theta$, the convolution integral in equation (39) is then dominated by frequencies very close to the target frequency (within $\delta\omega \sim 1/\Theta$), and one can then, to a good approximation, remove the relatively slowly varying factor $P_\psi c_\alpha c_\beta$ from within the integral to obtain

$$\langle|\tilde{\kappa}(\omega)|^2\rangle = N\left[\frac{\bar{n}P_\psi(\omega)}{4} + \langle\gamma_1^2\rangle\right], \quad (40)$$

where we have invoked Parseval's theorem, and $\bar{n} = N/\Theta^2$ is the mean number density of galaxies per steradian. To obtain our final estimate of the power, we subtract the shot noise term to obtain $\hat{P}_\psi(\omega) = 4(|\tilde{\kappa}|^2 - N\langle\gamma_1^2\rangle)/N\bar{n}$ and then average these estimates over a shell of frequencies in ω-space with some width $d\omega = \omega\, d\ln\omega$.

It is worth noting at this point that if we replace c_α in equation (38) by $c'_\alpha = (\sin 2\varphi, -\cos 2\varphi)$, or equivalently, if we apply the 90° rotation $(\gamma_1, \gamma_2) \to (\gamma_2, -\gamma_1)$ to the shear estimates, then the estimated power should vanish (aside from statistical noise). This is a reflection of the fact that while a general shear field has 2 real degrees of freedom, only one of them is excited by lensing. Using c_α in equation (38) effectively projects out the active component, while c'_α projects out the sterile component. This "rotation test" provides a useful check on the integrity of the data, as most sources of spurious image polarization would be expected to excite both components. For further discussion of this see Kaiser et al. (1994) and Stebbins (1996).

To estimate the uncertainty in $\hat{P}_\psi(\omega)$ we need to make some further assumptions about the density fluctuations. We shall assume that the real and imaginary parts of $\tilde{\kappa}(\omega)$ approximate a pair of Gaussian random fields. This is certainly appropriate for density fluctuations arising from inflation, but is also a very good approximation for many highly non-Gaussian (in real space) processes. An example is a shot noise process in which, even for a quite modest number of shots (e.g., 5 or so), the transform of the shots becomes quite accurately Gaussian as a consequence of the central limit theorem (see Kaiser and Peacock 1992 for illustrative examples). The Gaussian (transform) approximation is also valid for density fields that are non-Gaussian because of either nonlinear gravitational evolution or biasing. Under this assumption we can calculate the two-point function for the "raw" power $\langle\tilde{\kappa}^2(\omega)\tilde{\kappa}^2(\omega+\Delta\omega)\rangle$ and hence obtain the uncertainty in the shell-averaged power. For a filled square survey, the two-point function of the power is, like $|n(\omega)|^2$, a rather compact function with width $\delta\omega \sim 1/\Theta$, so estimates of the power at wavenumbers separated by more than $\delta\omega$ are statistically independent and computing the variance in the power averaged over some shell becomes essentially a counting exercise. One computes dN_ω, which is the effective number of independent modes, and then divides the mean power (signal + shot noise) by $(dN_\omega)^{1/2}$ (see Feldman, Kaiser, & Peacock 1994 for an application of this method to galaxy clustering in the QDOT redshift survey).

For a simple filled square–survey geometry the number of independent modes in each shell is just

$$dN_\omega = \frac{\pi\omega^2 d\ln\omega}{(\delta\omega)^2} , \quad (41)$$

where $\delta\omega = 2\pi/\Theta$ is the fundamental frequency. Assuming zero signal, one obtains a statistical uncertainty in $\Delta_\psi^2 \equiv \omega^2 P_\psi(\omega)/(2\pi)$ resulting from random intrinsic ellipticities of

$$\sigma(\Delta_\psi^2) = \langle(\Delta_\psi^2)^2\rangle^{1/2} = \frac{4\langle\hat{\gamma}_1^2\rangle\omega\Theta}{N(\pi d\ln\omega)^{1/2}} . \quad (42)$$

As noted in K92, for high-Z sources the statistical uncertainty is very small compared to the expected signal. For example, with $n \sim 2\times10^5$ galaxies per square degree and $\langle\gamma_1^2\rangle^{1/2} \sim 0.40$ (as obtained from typical cluster lensing studies for integrations of a few hr on a 4 m–class telescope) and for frequency resolution of, say, $d\ln\omega = \frac{1}{4}$, or four bins of power per log interval of frequency, we obtain $\sigma(\Delta_\psi^2) \simeq 1.15\times10^{-6}(2\pi\omega/\Theta)$, which is shown as the straight line in Figure 5 for a survey of side $\Theta = 3°$.

3.4.2. *Sampling Strategy*

The measurement noise estimate, equation (42), is a tiny ($\sim$1%) fraction of the power for our fiducial 3° survey field (assuming Peacock's estimate of the power), so one would expect, in such a survey, to detect the power at something like the $\sim$100 σ level. This is very nice. However, it does *not* imply a similar precision in determining the true mean universal power. For low spatial frequencies the uncertainty in the ensemble average power will be dominated by the fact that we only have a small number of independent modes. For a 3° survey the fundamental frequency is $\delta\omega \sim 120$, and the fractional uncertainty in $P_\psi(\omega)$ at, say, 2 $\delta\omega$ would be around 50%, rather than 1%. This sampling uncertainty is shown as the error bars in Figure 5 and clearly dominates over the measurement noise.

The situation here is very similar to that in galaxy clustering studies from redshift surveys, where, even though one might have a sample of many thousands of galaxies, the number of independent structures on the largest scales is quite small. In this situation one can measure the power in one's sample volume to extremely high precision, yet the value need not be representative of the ensemble average power spectrum. Whether this sampling uncertainty is relevant depends on that for which one wants to use the data. One useful application of redshift surveys is to apply the cosmic virial theorem and to obtain an estimate of the Ω of matter clustered like galaxies. This essentially involves taking the ratio of the pairwise velocity dispersion to the galaxy clustering amplitude (Davis & Peebles 1983). Both of these statistics may have large sampling noise, but their *ratio* (under the assumption that there is a universal mass per galaxy) is not affected by this. Similarly, in weak lensing

one can perform a cross-correlation between the shear of the faintest galaxies and the surface number density of somewhat brighter galaxies [chosen so that their $n(z)$ peaks roughly halfway to the background galaxies] to obtain an estimate of the mass-to-light ratio (K92). As with virial analysis, this does not involve the sample variance, and M/L can be measured to extremely high precision using a filled survey. If, however, one's goal is to use $P_\psi(\omega)$ to distinguish between, e.g., the three models shown in Figure 5, then the sampling noise is clearly a serious handicap.

As with galaxy clustering, sparse sampling (Kaiser 1986) could be quite helpful here. Imagine that one is to observe a similar number of galaxies, but with N_f sparsely spaced fields of size Θ_f scattered over a much larger square (of side Θ, as before). The function $|n(\omega)|^2$, which should be thought of as an instrumental point-spread function through which we measure the power, will now be much narrower (by a factor $\sim f^{1/2}$, where f is the areal filling factor of one's survey). This has two benefits: First, the fundamental frequency would decrease, so one would be able to probe beyond the peak in the spectrum (clearly an interesting and cosmology-dependent attribute). Second, in each region of frequency space one will obtain $1/f$ times as many independent estimates of the power, so the sampling uncertainty decreases by a factor $1/f^{1/2}$, which can be a considerable gain.

There is a price paid, however, for this increased resolution and precision, which is "aliasing." For a sparse survey the convolving kernel $|n(\omega)|^2$ will now have sidelobes in addition to the central peak that extend to relatively high frequencies $\omega_f \sim 2\pi/\Theta_f$, and our power estimator $|\tilde\kappa(\omega)|^2$ will in general contain some contribution from $\omega' \neq \omega$. The structure of the sidelobes depends on how one lays out one's fields. If this is done in a random or semirandom manner (perhaps by choosing a set of fields that avoid bright foreground objects), then the sidelobes look like (the square of) a random Gaussian field, smoothed on a scale $\delta\omega$, and the mean strength of the sidelobes is suppressed by a factor $\sim 1/N_f$, as compared to the central peak. If the fields are laid out on a grid, then the sidelobes are as strong as the central lobe but are spaced on a grid of spacing $N_f^{1/2}\delta\omega$ and cover only a fraction f of the frequency plane. Some examples are shown in Figure 6.

There are two aspects to the "aliasing problem"; the first is the mixing of power from frequencies similar to the target frequency: $\omega' \sim \omega$. For a random or gridlike survey this is small, provided $N_f \gg \omega^2\Theta^2$. This condition says that one must sample several fields per wavelength of interest. If the fields are laid out in a line, a substantial mixing of power is unavoidable (as is the case for pencil-beam or two-dimensional redshift surveys). This is not absolutely disastrous, as one can always convolve one's theoretical predictions, but it seems an unwanted and unnecessary complication, and we would discourage this. Also, in order to apply the rotation test described above, it is necessary that one have proper two-dimensional sampling and that the above condition be satisfied.

The second aspect is aliasing of power from higher frequencies $\omega' \gg \omega$. This is somewhat more model dependent, as it depends on how the power varies with frequency. One finds from equation (39) that the aliased power will be small compared to the power one is measuring from the target frequency, provided that $N_f \gg \omega^2\Theta^2\Delta_\psi^2(\omega')/\Delta_\psi^2(\omega)$. This again is physically reasonable; $N_f/(\omega^2\Theta^2)$ is the number of fields per square target wavelength, so when this condition is only marginally satisfied, the small-scale power induces a "root-N" contribution in the low-$\omega\kappa$ estimate that is equal to the intrinsic low-frequency κ fluctuations. Thus, if $\Delta_\psi^2(\omega)$ increases strongly toward small scales, then one would want to increase the sampling density. However, if the models shown in Figure 5 are a realistic guide, Δ_ψ^2 is actually falling with increasing frequency, so aliasing from small scales would not be a serious problem, and a rather sparse sampling would pay great dividends with little or no cost. It may be that this is overly optimistic, since, as mentioned above, nonlinearity may boost the power at small scales at late times and cause the predictions shown in Figure 5 to underestimate the lensing power. Nonetheless, it should still possible to choose N_f so as to make the aliased power small. Assuming that these conditions have been met, the power estimate is

$$\hat P_\psi(\omega) = \frac{4\Theta^2}{N^2}\left(|\tilde\kappa|^2 - N\langle\gamma_1^2\rangle\right), \tag{43}$$

and the uncertainty in the distortion power per log interval of wavenumber is given by

$$\sigma(\Delta_\psi^2) = \left(1 + \frac{NP_\psi}{4\Theta^2\langle\gamma_1^2\rangle}\right)\frac{4\langle\hat\gamma_1^2\rangle\omega\Theta}{N(\pi\, d\ln\omega)^{1/2}}\,. \tag{44}$$

(If there is insufficient rejection of high-frequency fluctuations, one will need to estimate and then subtract an extra constant term from eq. [43], and there would also be an additional contribution to eq. [44] from the fluctuations in the aliased power.) The two terms in equation (44) have opposite dependence on the overall survey size Θ, and the optimum choice (assuming a fixed instrument and integration time) is when these two contributions are equal: $\Theta_{\rm opt} = (NP_\psi/4\langle\gamma_1^2\rangle)^{1/2}$. For high-redshift sources and for large N, this would dictate a very sparse sampling indeed: $f = 4\langle\gamma_1^2\rangle/(nP_\psi) \sim 10^{-2}$ for $n \sim 2\times 10^5$ per square degree and $Z_s \sim 3$, but if one also wants to use the same survey to measure the shear for brighter and nearer objects, one should adopt a correspondingly less sparse strategy. As a specific example, if one were to spread one's fields over a square 3 times wider than the filled survey, then the sampling uncertainty would decrease by a factor of 3, while the shot-noise term would increase by a factor of 3. For $Z_s \simeq 3$ the former would still dominate, at least on large angular scales, and the resulting uncertainty is shown in Figure 5 as the error bars attached to the Λ-model spectrum. As one can see, the sparse sample has considerable improved precision, and one also has better coverage of the behavior of $P_\psi(\omega)$ around the peak, as the fundamental frequency is now reduced by a factor of 3 as well. To design a truly optimal survey for large-scale structure, one really needs to know the true level of small-scale power, so it would be prudent to perform a smaller scale filled survey first to establish this empirically.

3.4.3. *LSS and Amplification*

To close this discussion of large-scale structure, we consider what extra information can be gleaned from estimates of the surface density derived from the amplification. In general, we expect the rms convergence to be equal to the rms shear, and the convergence can be measured directly, as it causes a modulation of the counts of faint galaxies $\Delta n/n = -2(1-\alpha)\kappa$, where $\alpha = d\ln N(>l)/d\ln l = 2.5\ d\log$

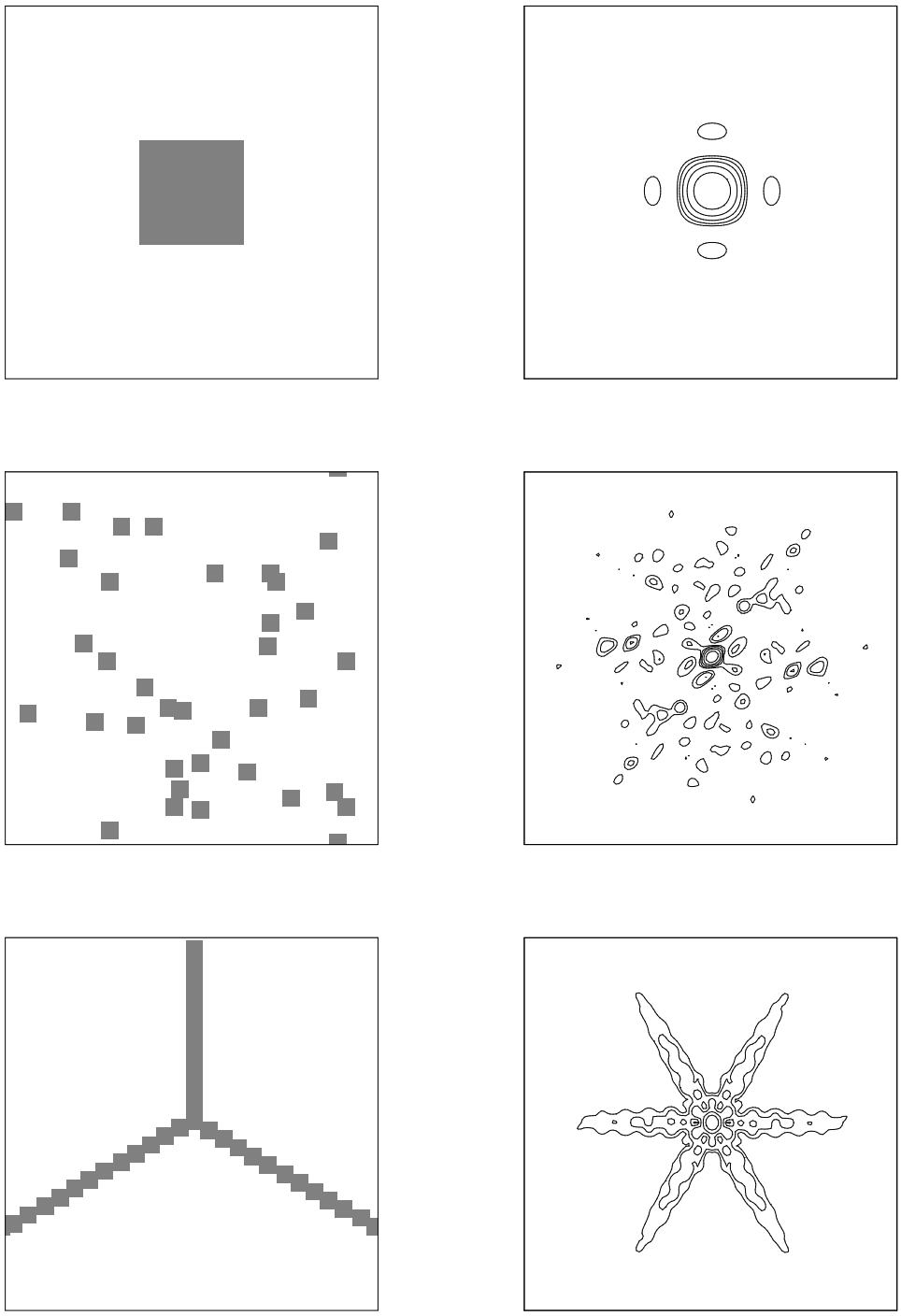

FIG. 6.—Left panels illustrate three possible survey geometries, containing $N_f = 36$ fields of 0.°5 in size (the box here is 10° on a side). The panels on the right show the corresponding point-spread functions for power spectrum estimation. The contours are logarithmic at 2^{-n} times the peak value. The filled survey has a wide central lobe and hence very poor precision, as the sampling of the power spectrum is very coarse (see text), but the aliasing of high frequencies is very small. The random sparse survey has a very tight central lobe and would yield a factor ~ 3 improvement in precision over the filled survey. There is also rather good rejection of neighboring frequencies close to the target frequency, but one can see the sidelobes (the typical height of which is suppressed by a factor $1/N_f$ relative to the central lobe) that extend to frequencies on the order of the inverse field size. For the models discussed here, however, the power aliased through these sidelobes would be very small. The "Y-beam" survey has relatively inferior performance: the sidelobes are at least as strong as for the random sparse survey, but the central lobe is much wider, giving relatively poor precision. Moreover, there is poor rejection of frequencies close to the target frequency, so the measured power spectrum at low frequencies will be quite distorted, and one would need to apply deconvolution.

N/d mag is the logarithmic slope of the counts, and the factor $-2(1-\alpha)$ is known as the "amplification bias factor." (See Broadhurst, Taylor, & Peacock 1995 for a detailed discussion, and Bartelmann & Narayan 1995, who have discussed the possibility of measuring the amplification from the modulation of the mean size of galaxies as a function of surface brightness.) At the magnitudes relevant for weak-lensing observations, $d \log N/d$ mag $\simeq 0.3$ (we will discuss the dependence of α on wave band and color presently), so large-scale structure will give rise to apparent clustering of galaxies on the sky with amplitude $\Delta n/n \simeq -0.5\kappa$.

For a power-law spectrum of mass fluctuations in an Einstein–de Sitter cosmology, the variance in κ grows as $\bar{z}^{1-n}$, where $\bar{z}$is the mean comoving distance to the background galaxies [here $z = 1 - (1 + Z)^{-1/2}$]. On the other hand, if galaxies are unbiased tracers of the mass, then $w(\theta)$ from the intrinsic spatial clustering decreases as $(1 - \bar{z})^4 \bar{z}^{-(3+n)}$ (K92), so, in this model, the relative importance of the lensing-induced clustering grows rapidly with increasing source redshift, and there is a crossover at $Z_s \sim 2$, beyond which the induced clustering comes to dominate (K92; Villumsen 1996b). As discussed above, however, a mass-traces-light normalization seems untenable for a high-Ω_m universe, and in either a low-Ω_m universe or a biased $\Omega_m = 1$ universe, the expected induced clustering is subdominant. In any case, it is not entirely clear how one can separate the two effects observationally (without accurate redshift information).

Another possibility is to cross-correlate the surface density κ derived from lensing of faint galaxies with the surface brightness for a sample of brighter objects [chosen so that their $n(z)$ peaks where the $g(z)$ for the fainter background galaxies peaks]. The procedure for doing this with κ derived from the shear was described in K92, but this can equally well be done with κ derived from the amplification. There is a slight complication here, in that the predicted effect is an anticorrelation of background and foreground galaxy counts (as the bias factor is negative), and this will be diluted (and perhaps overwhelmed) by contamination of the "background" sample by faint foreground galaxies, so an accurate knowledge of the luminosity function is needed to account for this properly.

For realistically normalized models we find rms $\kappa \sim 1\%$ on degree scales (for $Z_s \sim 3$). For a shear-based surface density estimate κ_γ the uncertainty is $\sigma(\kappa_\gamma) \simeq (\langle \gamma_1^2 \rangle / N)^{1/2} \simeq 0.4/N^{1/2}$, and it is much less than the expected signal for a survey like that discussed above. The uncertainty in the amplification-derived surface density is $\sigma(\kappa_A) = 0.5(1 - \alpha)^{-1}[(1 + nP_g)/N]^{1/2} \simeq 2[(1 + nP_g)/N]^{1/2}$, where P_g is the power spectrum of galaxy clustering, which can be (1) the angular power spectrum, in which case n should be the density of sources on the sky; or (2) the spatial power spectrum, in which case n should be the three-dimensional number density, the result being the same. The ratio of the statistical uncertainty for the two techniques is

$$\frac{\sigma(\kappa_A)}{\sigma(\kappa_\gamma)} = 2\left(\frac{1 + nP_g}{\langle \gamma_1^2 \rangle}\right)^{1/2} \simeq 5(1 + nP_g)^{1/2} . \qquad (45)$$

The factor $1 + nP_g$ [sometimes referred to as $\sim(1 + 4\pi n J_3)$] is an effective clustering multiplicity. For a distribution of randomly placed clusters, it is just the number of galaxies per cluster, and quite generally, the factor nP_g tells us by how much the variance of counts of galaxies exceeds that for a Poisson distribution.

For a power-law angular correlation function $w(\theta) = w_0(\theta/\theta_0)^{-0.8}$, which seems to be a reasonable fit to the data, $nP \simeq 0.8(k\theta_0)^{-1.2} 2\pi n w_0 \theta_0^2$. There are now a number of empirical estimates of $w(\theta)$ for faint galaxies that we can use to estimate $2\pi n w_0 \theta_0^2$. The following are some recent estimates (with $\theta_0 = 1'$): 1.52 (Couch, Jurcevic, & Boyle 1993); 1.1, 1.6 (Roche et al. 1993); 1.45 (Pritchet & Infante 1992); 1.74 (Efstathiou et al. 1991); 3.8 (Villumsen, Freudling, & da Costa 1996); 1.59 (Brainerd et al. 1995). While these estimates span quite a range of magnitude limits (the number density varying from ~ 10 arcmin^{-2} for the brighter surveys to ~ 400 arcmin^{-2} for the Hubble Deep Field), the estimates of $2\pi n w_0 \theta_0^2$ are very stable and indicate $nP \sim 2(\omega 1')^{-1.2}$. These results are discouraging in the extreme. Even on subarcminute scales, where the clustering becomes negligible, the noise in the surface density inferred from amplification is already about 5 times that for the shear-based κ estimates (so the extra information contained in the amplification is meager), and on larger scales the situation rapidly deteriorates. For cluster lensing, where one is probing structure on a scale $\sim 5'$–$10'$, and where it might have been hoped that amplification might resolve the "mass-sheet degeneracy" problem (Falco, Gorenstein, & Shapiro 1985; Schneider & Seitz 1995), clustering has already inflated the uncertainty by a factor of 2 or so; therefore a cluster like A1689, which can be detected at the 10 σ level in the shear, would only be detectable at the ~ 1 σ level (i.e., the diminution of the counts from lensing is about equal to the rms fluctuation expected from galaxy clustering alone). Worse still, for the degree scales of interest here, $\omega \sim 100$ rad$^{-1} \sim 0.03$ arcmin^{-1}, and we expect nP to have grown to around 120, so the clustering fluctuations exceed the Poisson fluctuations by about an order of magnitude. We reach a very similar conclusion if we use Peacock's linearized estimate of P, which is not surprising, as this power spectrum model is designed to fit the empirical data. Thus, on degree scales, one would expect $\sigma(\kappa_A) \sim 50\sigma(\kappa_\gamma)$; therefore, the extra information in the amplification-based κ estimate is negligible, and for surveys of the scale envisaged here, one would expect at best a marginal detection of the effect. The relatively high precision allowed by the shear-based surface density estimate relies on the assumption that the intrinsic shapes of galaxies are uncorrelated and could be compromised if in fact there are strong intrinsic alignments of galaxies on supercluster scales. There have been a number of attempts to detect correlated orientations of galaxies in superclusters—with the hope of distinguishing between "top-down" and "bottom-up" structure formation scenarios—but no convincing positive detections have been obtained (see Djorgovski 1986 for a review), and there are no indications from weak-lensing observations (from, e.g., the rotation test) of any intrinsic alignments at problematic levels.

The counts slope is somewhat wave band dependent (the counts in I are slightly flatter and those in V somewhat steeper than we have assumed). This might suggest that one should use the redder passband, and it has been suggested (Broadhurst 1996) that one would do better by selecting only red galaxies, as they have an even shallower counts slope and hence a larger (negative) amplification bias. However, this does not help here, as it now appears that faint red galaxies lie at relatively low redshift, compared to their bluer cousins (Luppino & Kaiser 1997), and this outweighs the gain from the flatter slope. It is somewhat unfortunate, though not entirely coincidental, that the most distant objects (the faint and blue galaxies) that suffer the greatest amplification have a very small amplification bias.

4. CLUSTER LENSING

We now consider lensing by an individual cluster that is assumed to dominate over the effect of foreground and background clutter. The goals here are to see the extent to which lensing-inferred mass-to-light ratios are dependent upon the assumed background cosmology and also to

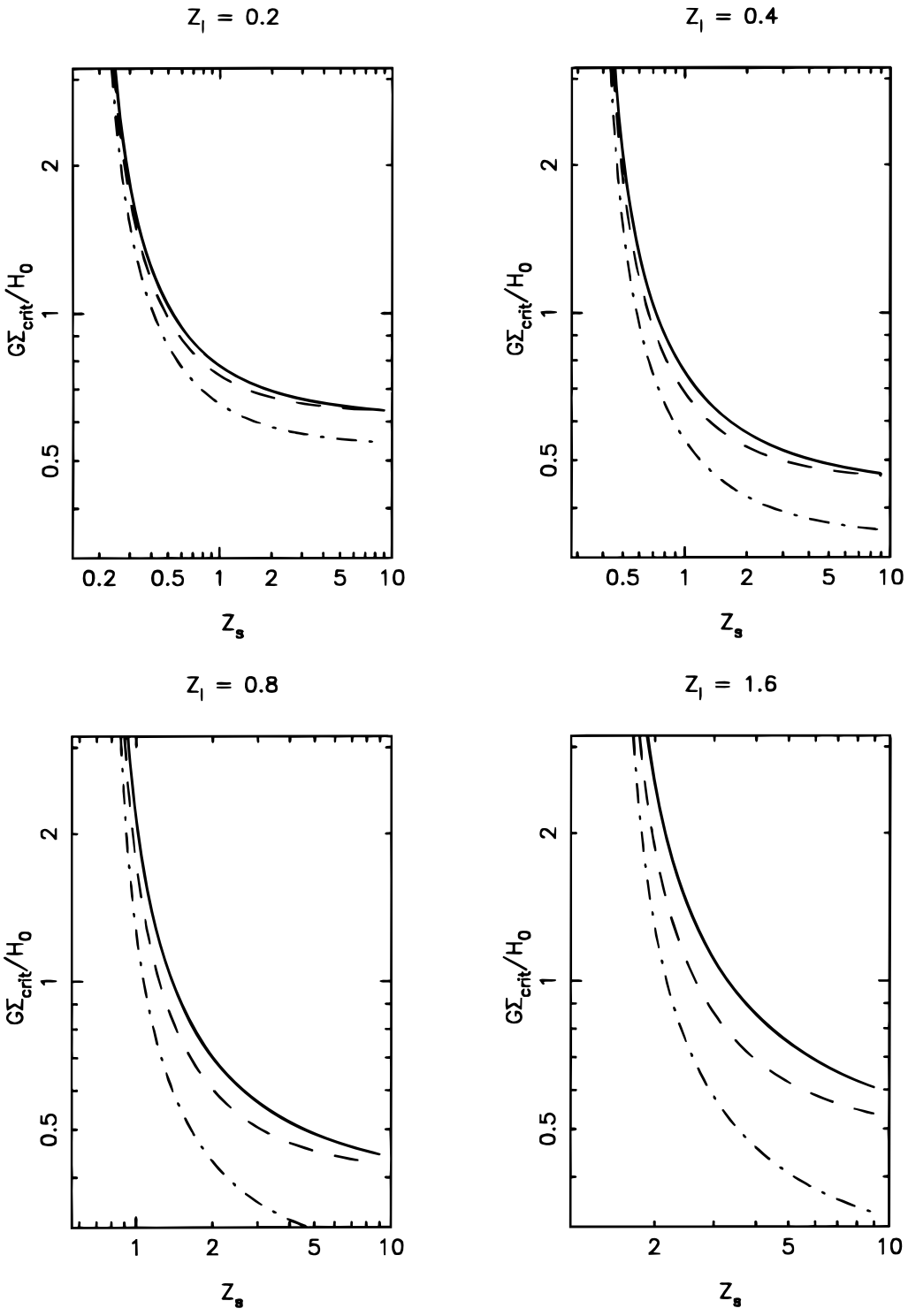

FIG. 7.—Critical surface density vs. source redshift for various lens redshifts and for our three illustrative cosmological models

explore the extent to which the comparison of weak-lensing distortion and other mass diagnostics (X-ray temperature or velocity dispersion) are sensitive to the background cosmology.

From equation (13), and specializing to deflections occurring in a single plane, we can write

$$\kappa = \frac{\psi_{xx} + \psi_{yy}}{2} = \frac{\Sigma}{\Sigma_{\rm crit}}, \tag{46}$$

where Σ is the surface mass density and $\Sigma_{\rm crit}$ is the critical surface density

$$\Sigma_{\rm crit} = \frac{H_0 \sqrt{1 - \Omega_0}(1 + Z_l) \sinh z_s}{4\pi G \sinh z_l \sinh (z_s - z_l)}, \tag{47}$$

which we have plotted against source redshift for a variety of lens redshifts in Figure 7.

For low Z_l the impact of cosmology is very weak, regardless of source redshift, but for $Z_s \sim 1$ or higher we find a

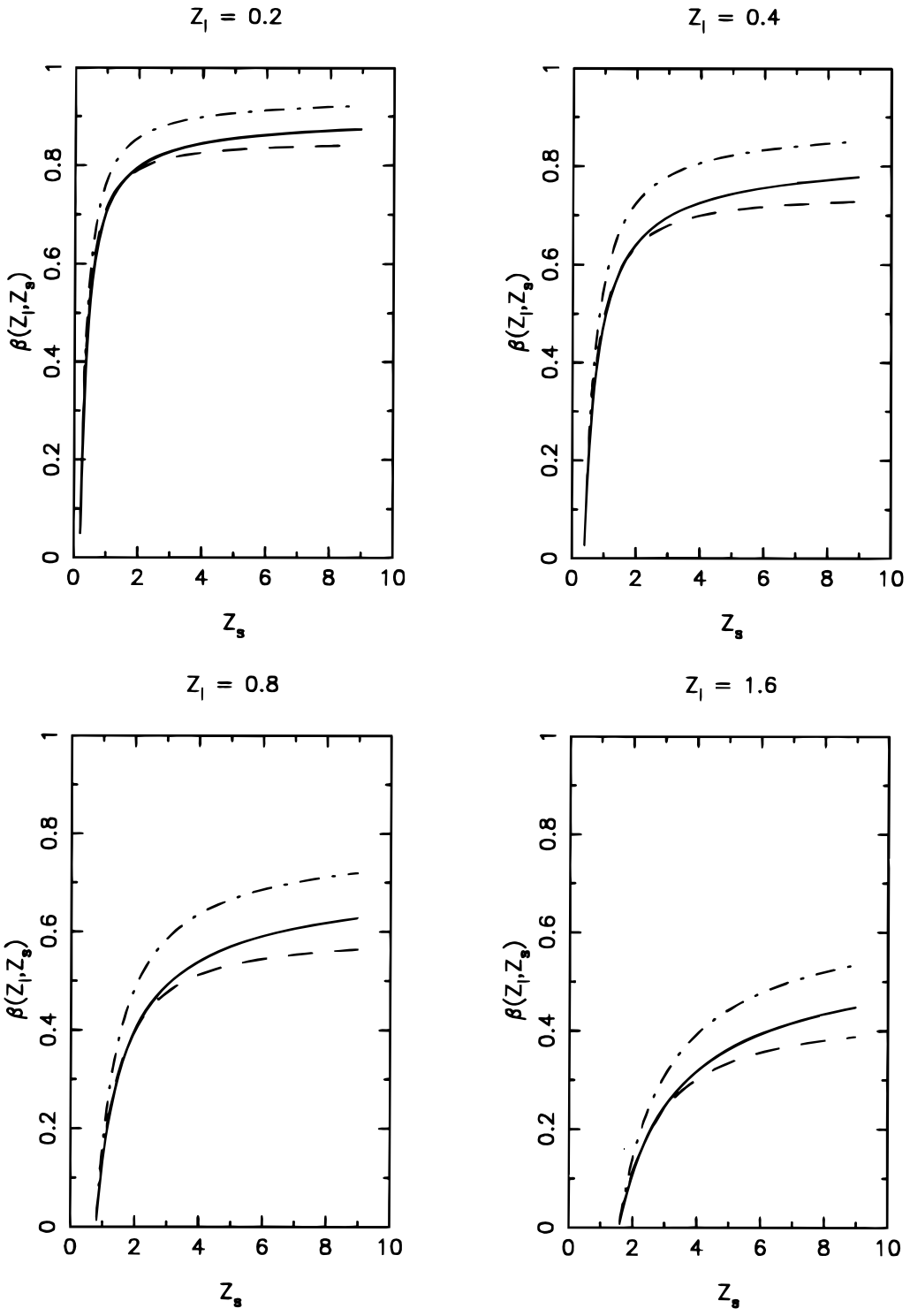

FIG. 8.—Relative distortion strength parameter β vs. source redshift for various lens redshifts and for various values of Ω_0

significant reduction in $\Sigma_{\rm crit}$ in the Λ-dominated model (owing to the increased path length), and an observer living in such a universe but using the EdS $\Sigma_{\rm crit}$ would overestimate the mass of a cluster at $Z \sim 1$ by almost a factor of 2.

Thus, in the interpretation of what weak-lensing observations of clusters at this redshift imply for, e.g., the background galaxy redshift distribution, cosmological factors can have a considerable impact.

It is also interesting to compare the mass inferred from lensing to that obtained from virial analysis and/or X-ray temperature information. Virial analysis gives

$$\Sigma = \frac{\alpha\sigma^2}{G\theta a(z_l)\sinh z_l} = \frac{\alpha H_0\,\sigma^2(1-\Omega_0)^{1/2}(1+Z_l)}{G\sinh z_l}, \quad (48)$$

where α is some number of order unity that accounts for the radial profile of the cluster, velocity dispersion anisotropy, departures from sphericity, departures from equilibrium, substructure, mass/light segregation, etc., so assuming that this can be done to sufficient accuracy, we should find

$$\frac{\kappa\theta}{4\pi\alpha\sigma^2} = \beta(z_l, z_s) = \frac{\sinh(z_s - z_l)}{\sinh z_s} . \quad (49)$$

This dimensionless ratio is directly observable, and, assuming that the lens and background galaxy redshifts are also known, is dependent only on the cosmological model. To see how useful this is, in Figure 8 we have plotted β as a function of Z_l, Z_s for the three fiducial cosmological models. It is clear that the effect of varying the cosmological parameters on this quantity is very weak.

Thus, even if one were to succeed in determining the redshift distribution for the background galaxies and in quantifying the systematic errors in virial and X-ray mass measurements alluded to above, the prospect for extracting useful cosmological information from this test is not very bright.

5. SUMMARY

The main new analytic result of this paper is equation (25), which gives the angular power spectrum of the distortion in terms of the three-dimensional power spectrum of potential fluctuations [a somewhat more useful form for predicting $P_\psi(\omega)$ from models for the density-contrast power spectrum P_δ is given in eq. (34)]. We have used this to compute the distortion power for a number of illustrative models.

Note that while we have invoked linear perturbation theory for the evolution of the power spectrum in the various illustrative models, the relation (25) is quite general and applies equally well to linear or nonlinear density fluctuations, and it does not make any assumption regarding the Gaussianity or other qualities of the mass density structure in our universe.

We have shown that for a sharply peaked three-dimensional spectrum, the scale on which the distortion appears is cosmology dependent, being up to a factor of ~ 2 smaller in low-density models. This is reflected in the model predictions shown in Figure 5 based on Peacock's models for $P(k)$, which has a kneelike feature at $\lambda \sim 100\ h^{-1}$ Mpc, and consequently the location of the corresponding peak in $P_\psi(\omega)$ is cosmology dependent. A more powerful cosmological discriminator is the growth of the distortion with redshift, this being stronger in low–matter density models in general and in Λ-dominated models in particular. This requires that one have at least approximate estimates of the redshift of the faint galaxies as a function of flux, but this should be feasible using approximate redshift estimates by fitting multicolor photometry to template spectra (Loh & Spillar 1986; Conolly et al. 1995; Sawicki, Lin, & Yee 1996). This cosmological test does not require any external normalization of the power spectrum, but it does require that we be able to measure the distortion with sufficient precision at both high and low redshift.

The most promising application of this test is to constrain Ω, as the distinction between the different low-density models is relatively weak compared to the distinction between high- and low-density parameters.

One can also ask whether one can hope to pin down the cosmology by making use of external normalization. This is certainly possible in principle, but it is not yet entirely clear what is the appropriate normalization. Bernardeau et al. (1996) normalized to a fixed amplitude for the density contrast and consequently found a very strong dependence of the predicted shear on the matter density: $P_\psi \propto \Omega_m^{1.5}$ or thereabouts. We have argued that this normalization is unrealistic. If instead we normalize to galaxy clustering with a scale-invariant bias and mass-to-light ratio fixed by small-scale cosmic virial theorem analysis, then we reach the opposite conclusion: low–matter density models in general and Λ-dominated models in particular then predict much stronger distortion at high redshift (the distortion being cosmology independent for low redshift). If, on the other hand, one were to normalize to some value for the amplitude of large-scale bulk flows (still unfortunately a rather uncertain quantity), then $P_\psi \propto \Omega_m^{0.8}$ for very low source redshift, but for $Z_s \sim 1$–3 and for realistic spectral indices n around -1 to -2, the predicted distortion is only very weakly cosmology dependent. A very similar result is obtained if one normalizes to cluster abundances. This weak dependence on cosmology was also apparent when we computed the distortion power for Peacock's fit to galaxy clustering data, where all three illustrative models agree in distortion power to within a factor of 2. The high-density model assumed a rather mild bias $b = 1.6$, and for stronger bias the difference between the models would be even less.

With a realistic normalization we predict rms shear at the $\sim 1\%$ level at degree scales for sources at $Z_s \sim 3$, which should be detectable at the $\sim 100\ \sigma$ level with a survey covering ~ 10 deg^2 (which would contain $\sim 2 \times 10^6$ galaxies). We found, however, that for a filled survey of this size, the sampling uncertainty would much larger than the measurement noise, particularly at the largest scales, which in some ways are the most interesting. For some applications the sampling uncertainty is irrelevant, but for the tests described above it is a serious handicap. The sampling noise can be reduced considerably by adopting a sparse sampling strategy (at some small cost in increased measurement noise). An important constraint on the design of such sparse surveys is aliasing of power from small scales. While in principle this can be measured and subtracted to obtain a fair estimate of the true large-scale power, it is still an unwanted complication, and, if the aliased power is dominant, the precision will be compromised. Peacock's empirically based models for the linear power spectrum predict very low power at high frequencies and would favor very sparse sampling (for deep surveys at least), but the safest approach is to measure the high-frequency power directly with a filled survey and to use this to determine the optimal sampling rate.

Finally, we considered the impact of cosmology on mass estimates for individual clusters. We found that the critical surface density was very similar in the matter-dominated models, but was considerably lower for high-redshift lenses in a Λ-dominated model. This is relevant to the result of Luppino & Kaiser (1997), who found a strong shear signal for the cluster MS 1054 at $Z_l = 0.83$. In a Λ-dominated model the mass for this cluster would be reduced by about 40%. We also explored how the ratio of the inferred dimensionless surface density to virial mass (or mass inferred from X-rays) depends on cosmology, but found this to be a very weak effect.

REFERENCES

Bar-Kana, R. 1996, ApJ, 468, 17
Bartelmann, M., & Narayan, R. 1995, ApJ, 451, 60
Baugh, C., & Efstathiou, G. 1994, MNRAS, 267, 323
Bernardeau, F., van Waerbeke, L., & Mellier, Y. 1996, astro-ph/9609122
Blandford, R. D., Saust, A. B., Brainerd, T. G., & Villumsen, J. V. 1991, MNRAS, 251, 600
Bonnet, H., Fort, B., Kneib, J-P., Mellier, Y., & Soucail, G. 1993, A&A, 280, L7
Bonnet, H., Mellier, Y., & Fort, B. 1994, ApJ, 427, L83
Brainerd, T., Blandford, R., & Smail, I. 1996, ApJ, 466, 623
Brainerd, T., Smail, I., & Mould, J. 1995, MNRAS, 275, 781-789
Broadhurst, T. 1996, preprint, astro-ph/9511150
Broadhurst, T., Taylor, A., & Peacock, J. 1995, ApJ, 438, 49
Cole, S., & Kaiser, N. 1989, MNRAS, 237, 1127
Connolly, A. J., Scabai, I., Szalay, A. S., Koo, D. C., Kron, R. C., & Munn, J. A. 1995, AJ, 110, 2655
Couch, W., Jurcevic, J., & Boyle, B. 1993, MNRAS, 260, 241
Dahle, H., Maddox, S., & Lilje, P. 1994, ApJ, 435, L79
———. 1998, in preparation
Davis, M., & Peebles, J. 1983, ApJ, 267, 465
Djorgovski, S. 1986, in Nearly Normal Galaxies, ed. S. M. Faber (New York: Springer)
Dyer, C., & Roeder, R. 1974, ApJ, 189, 167
Efstathiou, G., Bernstein, G., Katz, N., Tyson, J., & Guhathakurta, P. 1991, ApJ, 380, L47
Fahlman, G., Kaiser, N., Squires, G., & Woods, D. 1994, ApJ, 437, 56
Falco, E., Gorenstein, M., & Shapiro, I. 1985, ApJ, 289, L1
Feldman, H., Kaiser, N., & Peacock, J. 1994, 426, 23
Fort, B., Mellier, Y., & Dantel-Fort, M. 1997, A&A, 321, 353
Fort, B., Mellier, Y., Dantel-Fort, M., Bonnet, H., & Kneib, J.-P. 1996, A&A, 310, 705
Gunn, J. E. 1967, ApJ, 147, 61
Kaiser, N. 1986, MNRAS, 219, 785
———. 1987, MNRAS, 227, 1
———. 1992, ApJ, 388, 272 (K92)
———. 1995, ApJ, 439, L1
Kaiser, N., & Peacock, J. 1992, ApJ, 379, 482
Kaiser, N., & Squires, G. 1993, ApJ, 404, 441
Kaiser, N., Squires, G., Fahlman, G., & Woods, D. 1994, Proc. 29th Rencontre de Moriond, ed. F. Durret, A. Mazure, & J. Tran Thanh Van (Gif-sur-Yvette: Editions Frontières)
Limber, D. 1954, ApJ, 119, 655
Loh, E. D., & Spillar, E. J. 1986, ApJ, 303, 154
Luppino, G., & Kaiser, N. 1997, ApJ, 475, 20
Miralda-Escudé, J. 1991, ApJ, 380, 1
Mould, J., Blandford, R., Villumsen, J., Brainerd, T., Smail, T., Small, T., & Kells, W. 1994, MNRAS, 271, 31
Peacock, J. 1996, astro-ph/9608151
Press, W., & Schechter, P. 1974, ApJ, 187, 425
Pritchet, C., & Infante, L. 1992, ApJ, 399, L35
Roche, N., Shanks, T., Metcalfe, N., & Fong, R. 1993, MNRAS, 263, 360
Sawicki, M. J., Lin, H., & Yee, H. K. C. 1996, AJ, 113, 1
Schneider, P., & Seitz, C. 1995, A&A, 294, 411
Smail, I., & Dickinson, M. 1995, ApJ, 455, L99
Smail, I., Ellis, R., & Fitchett, M. 1995, MNRAS, 273, 277
Smail, I., Ellis, R., Fitchett, M., & Edge, A. 1994, MNRAS, 270, 245
Squires, G., Kaiser, N., Fahlman, G., Babul, A., & Woods, D. 1996b, ApJ, 469, 73
Squires, G., Kaiser, N., Fahlman, G., Woods, D., Babul, A., Neumann, D., & Bohringer, H. 1996a, ApJ, 461, 572
Stebbins, A. 1996, astro-ph/9609149
Strauss, M. & Willick, J. 1995, Phys. Rep., 261, 271
Tyson, J. A., Valdes, F., & Wenk, R. 1990, ApJ, 349, L1
Tyson, J. A., & Fischer, P. 1995, ApJ, 446, L55
Valdes, F., Jarvis, J. F., Mills, A. P., Jr., & Tyson, J. A. 1984, ApJ, 281, L59
Valdes, F., Tyson, J., & Jarvis, J. 1983, ApJ, 271, 431
Villumsen, J. V. 1996a, preprint, astro-ph/9512001
———. 1996b, MNRAS, 281, 369
Villumsen, J., Freudling, W., & da Costa, L. 1996, astro-ph/9606084
Webster, R. 1985, MNRAS, 213, 871
White, S., Efstathiou, G., & Frenk, C. 1993, MNRAS, 262, 1023